*Acta Oceanol. Sin.*, 2021, Vol. 40, No. 11, P. 162–175
https://doi.org/10.1007/s13131-021-1833-z
http://www.aosocean.com
E-mail: ocean2@hyxb.org.cn

# Tracking historical storm records from high-barrier lagoon deposits on the southeastern coast of Hainan Island, China

Liang Zhou[1, 2, 3], Xiaomei Xu[4], Yaping Wang[3], Jianjun Jia[3], Yang Yang[5], Gaocong Li[6], Changliang Tong[2], Shu Gao[2, 4*]

[1] School of Geography, Geomatics, and Planning, Jiangsu Normal University, Xuzhou 221116, China

[2] Hainan Key Laboratory of Marine Geological Resources and Environment, Haikou 570206, China

[3] State Key Laboratory of Estuarine and Coastal Research, East China Normal University, Shanghai 200046, China

[4] Ministry of Education Key Laboratory for Coast and Island Development, Nanjing University, Nanjing 210023, China

[5] School of Marine Science and Engineering, Nanjing Normal University, Nanjing 210046, China

[6] Department of Marine Technology, Guangdong Ocean University, Zhanjiang 524088, China

Received 5 February 2021; accepted 10 March 2021



**Abstract**

The relationship between storm activity and global warming remains uncertain. To better understand storm–climate relationships, coastal lagoon deposits are increasingly being investigated because they could provide high-resolution storm records long enough to cover past climate changes. However, site-specific sediment dynamics and high barriers may bias storm reconstructions. Here, we aimed to investigate these factors through the reconstruction of five distinct storm records (XCL-01, XC-03, XC-06, XC-07, XC-08) from different water depths in a lagoon with a high barrier (i.e., Xincun Lagoon of Hainan Island). Sediment cores were characterized using high-resolution grain size and XRF measurements, to identify storm events. These data were coupled with a numerical simulation to obtain bed shear stress data with high-spatial resolution to better understand storm-induced sediment transport mechanisms. $^{210}$Pb dating and Pb pollution chronostratigraphic markers indicated that the chronology of the storm deposit sequences of the cores span the period between 117 a and 348 a. The grain size and XRF results indicated numerous, highly variable and short-duration fluctuations, suggesting that storm-induced coarse-grained sediments were deposited at these core sites. The inconsistent storm events recorded in these cores suggest that these sites have different preservation potentials for storm deposits. However, the consistence between storm sediment records and historical documents for Core XCL-01 indicates that high-barrier lagoons could provide long-term storm event records with high preservation potential.

**Key words:** storm deposits, preservation potential, sediment dynamics, high-barrier lagoon, Hainan Island

**Citation:** Zhou Liang, Xu Xiaomei, Wang Yaping, Jia Jianjun, Yang Yang, Li Gaocong, Tong Changliang, Gao Shu. 2021. Tracking historical storm records from high-barrier lagoon deposits on the southeastern coast of Hainan Island, China. Acta Oceanologica Sinica, 40(11): 162–175, doi: 10.1007/s13131-021-1833-z

## 1 Introduction

Global warming is expected to increase the frequency and intensity of storm events in the future (IPCC, 2013). This issue has attracted wide social attention, because storms often trigger large waves and storm surges, which may severely affect coastal geomorphology (Wang et al., 2009; Almeida et al., 2012; Liu et al., 2019) and ecosystems (Greening et al., 2006; Zheng and Tang, 2007; Li et al., 2014; Chen et al., 2018), and may result in catastrophic losses of life and resources. However, the brevity of tide gauge records on the scale of several decades or incomplete historical records on the last centuries make the assessment of long-term trends in storm events difficult (e.g., Donnelly and Woodruff, 2007; Woodruff et al., 2009; Lane et al., 2011). Thus, the extraction of long-term storm information from sedimentary records is essential.

Previous paleostorm studies have widely been conducted in low energy environments (e.g., lagoons, lakes, and ponds). These environments, where the background sedimentation primarily by fine-grained sediments occurs, are usually protected by sand barriers (Liu and Fearn, 1993; Sabatier et al., 2008; Woodruff et al., 2009), which are very effective in trapping storm-induced coarse-grained sediments. Among them, back-barrier lagoons with low-lying barriers (top elevation lower than that of the local extreme storm surge) have been recognized as one of the most suitable environments to preserve overwash deposits of storm events, which has greatly improved the interpretation of the long-term evolution of coastal systems and the understanding of the response of intense storm activities to climatic changes (Sabatier et al., 2008; Switzer and Jones, 2008; Degeai et al., 2015; Rouina et al., 2016). Sand layers in lagoon deposits are con-

Foundation item: The National Natural Science Foundation of China under contract Nos 41706096 and 41530962; the Research Start-up Project of Jiangsu Normal University under contract No. 19XSRX006; the Opening Foundation of Hainan Key Laboratory of Marine Geological Resources and Environment under contract No. HNHYDZZYHJKF005; the High-level Talent Program of Basic and Applied Basic Research Programs (Field of Natural Science) in Hainan Province under contract No. 2019RC349; a project funded by the Priority Academic Program Development of Jiangsu Higher Education Institutions.
*Corresponding author, E-mail: sgao@sklec.ecnu.edu.cn

sidered to be related to storm overwash processes, in which storm surges and/or waves overtop the low-lying sand-barrier and transport coarse-grained materials into the back-barrier lagoon during storm passage. However, overwash processes may be prevented by high sand-barriers, especially when the back-barrier environment is blocked/surrounded by hills or high sand-barriers. This character may decrease the vulnerability of such lagoons to storm impacts (Li et al., 2006). However, whether these conditions have potential for the long-term reconstruction of storm events is poorly understood. Moreover, sediment dynamics in lagoons with high-barrier are relatively complex, which may hamper storm events reconstructions. The mechanisms of storm deposits formation in the back-barrier lagoon with high-barrier have not been fully understood. Thus, the potential effects of the sedimentary processes specific to each site may be a significant issue for the understanding of sedimentary records.

The Hainan Island is located in the northern part of the South China Sea (SCS), which is seriously affected by frequent storms during July to October (Ren et al., 2002; Fogarty et al., 2006). The Hainan Island coast is incised by numerous barrier lagoons with high sand barriers, particularly on the southeastern coast, which is characterized by a series of long, high sand barriers and barrier peninsulas (Wang, 1998). The long-term storm records of coastal lagoons with high-barriers and the sediment dynamics of such lagoons under the impact of storm activity have rarely been studied in the northern SCS. Jia et al. (2012) and Zhou et al. (2017a) have shown that coastal lagoon deposits of this region contain information on storm activities. These results indicate that lagoons with high barriers may be an important, and largely over-looked, resource of long-term storm event activities.

In this paper, we study the sedimentary dynamics of coarse-grained storm deposits in the high-barrier lagoon, and examine whether the sediment in the high barrier lagoon can be used to reconstruct long-term storm variations.

## 2 Study area

The Hainan Island is the largest island in the SCS. This island is influenced by a tropical monsoonal climate, and rainfall accompanied by frequent storms occurs from May to October. Annually, two storms cross the Hainan Island on average, with a maximum of around five events (Liang et al., 2015). The east coast is influenced by an irregular semidiurnal tide, with mean tidal ranges <1 m (Wang, 1998). Historical documents (Chen, 1995) and instrumental observations from the southeastern coast show no obvious evidence for tsunami activities.

The Xincun Lagoon (XC) is located on the southeastern coast

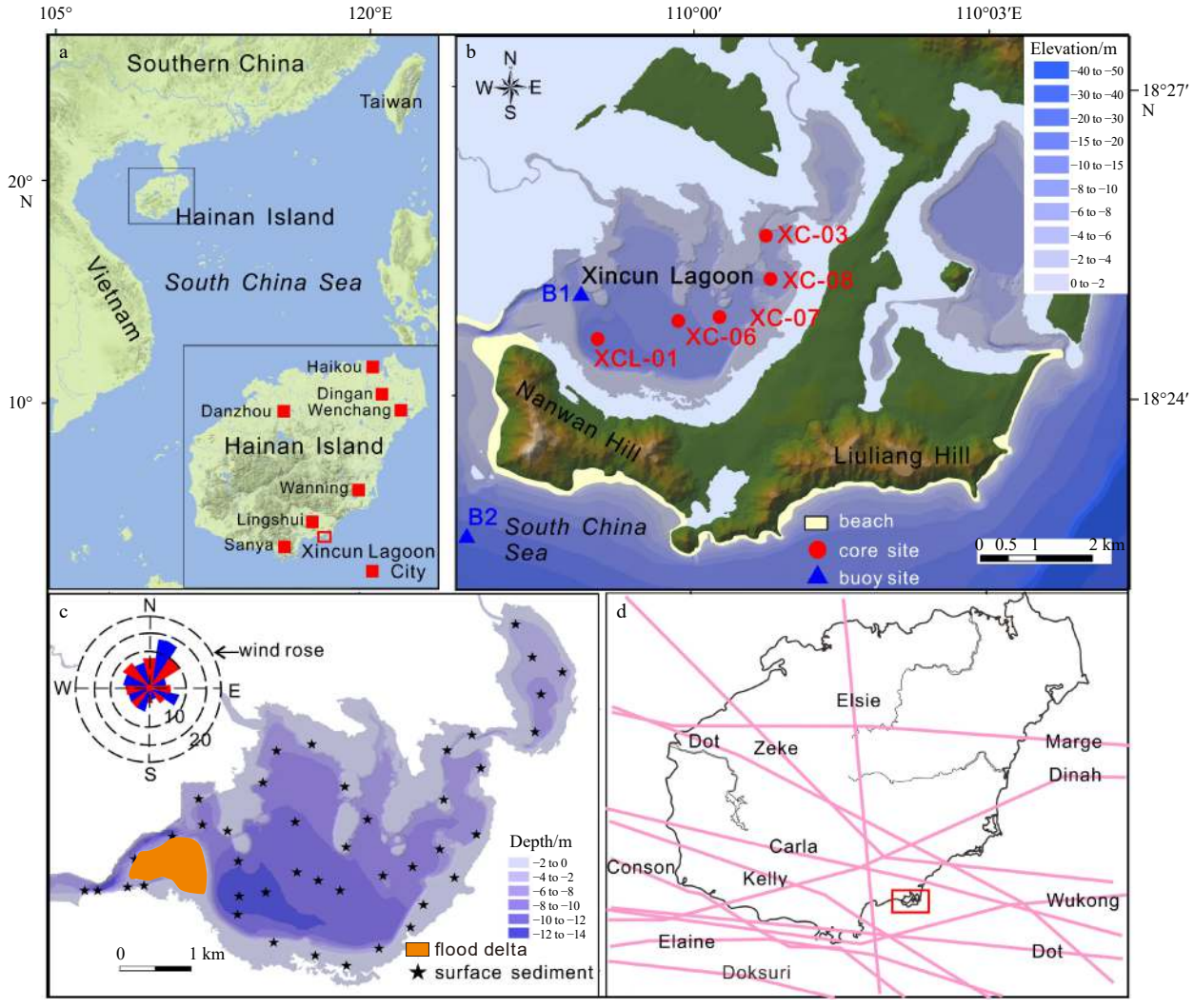


**Fig. 1.** Location of Xincun Lagoon on the southeastern coast of Hainan Island (a), core sites and tidal location in the Xincun Lagoon (b), surface sample location (c), and passage of major storm that impacted Xincun Lagoon since 1950 CE (d). The inset in c shows the wind direction rose map along Lingshui coast (date source: The Compile Committee of China Bay Record, 1999).

of Hainan Island (Fig. 1a), with a surface area of about 22 km$^2$. The mean water depth of the tidal basin is about 4.2 bmsl (below mean sea level) (Fig. 1b), and the deeper areas are distributed in the southwest of the lagoon, with maximum depth >12 m bmsl. Flood and ebb deltas are well developed (Fig. 1b). The spindle-shaped lagoon was formed in a transgression process in the Late Quaternary and is separated by granite hills (i.e., Nanwan Monkey Hill) from the SCS. The tide in this lagoon is irregularly diurnal (Gong et al., 2008). There is only one entrance (about 3.5 km long and 260 m wide) connecting the tidal basin to the SCS (Song, 1984). Under normal weather conditions, wind waves within the Xincun Lagoon are assumed to be negligible (with typical wave heights ranging from 0.3 m to 0.6 m; The Compile Committee of China Bay Record, 1999). Furthermore, the tidal current velocity in the tidal basin is not greater than 0.1 m/s (Gong et al., 2008; Yang et al., 2017) in the inner part of the lagoon. In addition, two small streams flow into the tidal basin with a very small discharge of <1 m$^3$/s (The Compile Committee of China Bay Record,1999). These destructive cyclonic storms tend to pass the Xincun Lagoon on its west (land) side; the wind direction switches from northwesterly to northeasterly in such a case (Fig. 1; Gong et al., 2008). Historical records document a history of intense storm occurrences on the southeastern coast, with known events such as in 1890, 1897, 1920, 1954, 1971, 1981 and 2000 (Chen, 1995; Table 1). Over the past 60 years, the highest storm water level was about 2.73 m asl (above sea level) in the Xincun Lagoon, which was recorded during the No. 8105 storm in 1981 (Chen, 1992).

## 3 Materials and methods

### 3.1 *Field investigation and sedimentary analysis*

Two detailed field investigation were conducted in the Xincun Lagoon in August 2013 and December 2015, respectively. Five short cores (XCL-01, XC-03, XC-06, XC-07, XC-08) were collected from this lagoon along the SW to NE (Fig. 1). These cores were transported to the State Key Laboratory of Marine Environmental Science of Xiamen University where they were split, described, photographed, and stored at 4°C until further analysis. Prior to sampling, high resolution (200–500 μm) depth profiles of the elemental composition of Core XCL-01 were measured using an Avaatech X-ray fluorescence core scanner following the method of Richter et al. (2006). Geochemical data were obtained at two tube voltage (10 kV and 30 kV; Richter et al., 2006).

Grain-size analysis was performed on a Mastersizer-2000 laser diffraction particle-size analyzer with an interval of 1 cm and a relative error below 3% for replicated measurements. Grain-size parameters (e.g., D90; D90 is the grain size at the cumulative volume of 90% from the smaller grain size side in the grain size distribution of the sediment grains) were determined using GRADISTAT v8 (Blott and Pye, 2001).

### 3.2 *Age dating*

The chronology of the cores was established using a combination of dating techniques including $^{210}$Pb dating, $^{137}$Cs dating, and Pb chronostratigraphic markers. For $^{210}$Pb activity, sediment cores XCL-01, XC-06, XC-07, and XC-03 were sampled following a regular 5 cm sampling interval, and then $^{210}$Pb activities were conducted on an HPGe Alpha-ray spectrometer. $^{137}$Cs activities in samples from cores XCL-01 and XC-08 were measured using Germanium ray spectrometry (ORTEC, GMX30P-A). $^{210}$Pb ages were calculated by the methods described in Jia et al. (2012) and Zhou et al. (2017b, 2021). Discrete ages for individual $^{210}Pb_{ex}$ measurement were determined using the constant initial concentration (CIC) model (Appleby and Oldfield, 1978).

### 3.3 *Hydrographic data and numerical modeling of storm currents*

Two buoys were deployed at a nearshore area near the Xincun Lagoon (B2) and the internal area of the lagoon (B1) prior to and after Typhoon Doksuri (2017) for a period of three weeks (Fig. 1). The two buoys continuously measured the tidal level and wave height. Typhoon Doksuri was a strong category 2 storm when it hit the southern coast of Hainan Island, and caused seriously damage (e.g., coastal erosion and property loess) along the southern and eastern coast of Hainan Island (www.typhoon.hainanqx). Wave height instruments were only deployed at the B2 location. The RBR XR-420-TG instrument was adopted to continuously measure the tide level at the two stations.

To estimate the bed shear stress in the Xincun Lagoon during Typhoon Doksuri, hindcast surge and wave modeling was carried out using the Delft3D coupled hydrodynamic-wave model, which calculate the wavefield, including the effects of currents and the storm surge. The model is commonly used for accurately simulating storm surges and wave growth with a set of input parameters (atmospheric pressure, storm track data; Hu et al., 2015; Bastidas et al., 2016). Surges were adapted to account for the position of the astronomical tide at landfall and expressed relative to the mean sea level datum.

**Table 1.** Major storm events impacting Lingshui coast between 1950 and 2014 (http://tcdata.typhoon.gov.cn; The Compile Committee of China Bay Record, 1999; Ying et al., 2014)

| Date | Name | Maximum wind/(m·s$^{-1}$) | Pressure/hPa | Category | Maximum tidal water level/m |
|---|---|---|---|---|---|
| 1954.05.11 | Elsie | 35 | 960 | 1 | 2.44 |
| 1962.09.21 | Carla | 35 | 984 | 1 | – |
| 1971.05.25 | Dinah | 35 | 990 | 1 | – |
| 1971.10.09 | Elaine | 45 | 975 | 2 | 2.60 |
| 1973.09.14 | Marge | 42 | 975 | 1 | – |
| 1981.06.04 | Kelly | 45 | 965 | 2 | 2.73 |
| 1985.10.21 | Dot | 40 | 970 | 1 | – |
| 1989.06.10 | Dot | 35 | 970 | 1 | – |
| 1991.07.13 | Zeke | 40 | 965 | 1 | – |
| 2000.09.09 | Wukong | 33 | 975 | 1 | – |
| 2005.09.26 | Damrey | 35 | 970 | 1 | – |
| 2010.07.16 | Conson | 35 | 970 | 1 | – |

Note:– means no data.

## 4 Results

### 4.1 *Lithostratigraphy*

Within Core XCL-01, sediment was mainly composed of a greyish sandy silt mixture, with many shell fragments. The sediments of cores XC-06, XC-07, and XC-08 consisted of clay-silt interbedded within a sand layers mixture with siliciclastic sand and shell fragments. The upper part of Core XC-03, consisted of light grey-brown organic-rich clay-silt, while the lower bed (below 20 cm depth) consisted of grey sand. A grey-white sand layer appeared at the depth of 30 cm, which was 2 cm-thick well-sorted grey sand.

### 4.2 *Age model*

#### 4.2.1 *$^{210}$Pb dating*

The sedimentation rates and the chronology of historical storm deposits were determined by cesium-137 ($^{137}$Cs) and lead-210 ($^{210}$Pb) dating methods.

There were mixed layers in the top 5–10 cm, which were followed by a normally exponential decaying region, and a background region of support $^{210}$Pb ($^{210}$Pb$_{ex}$) activities were detected among sediment cores XC-06, XC-07, XC-03 (Fig. 2). We extended the decaying trend lines of the $^{210}$Pb$_{ex}$ activities upward above the background region, and the average sedimentation rates of sediment cores XCL-01, XC-06, XC-07, and XC-03 were calculated to be 0.55 cm/a, 0.45 cm/a, 0.63 cm/a, and 0.27 cm/a, respectively. In Core XCL-01, there were relatively steady $^{210}$Pb activities below the depth of 61 cm, and the logarithms of excess $^{210}$Pb activities displayed a linear decline with depth, suggesting a relatively stable sedimentation rate of 0.55 cm/a (Fig. 2). These sedimentation rate results were similar to those of previous studies on the coastal embayment sediments of Hainan Island (Ge et al., 2003; Jia et al., 2012). However, the $^{137}$C activity in most core samples (e.g., XCL-01 and XC-08) was below the background value, and thus, we could not calculate an acceptable sedimenta-

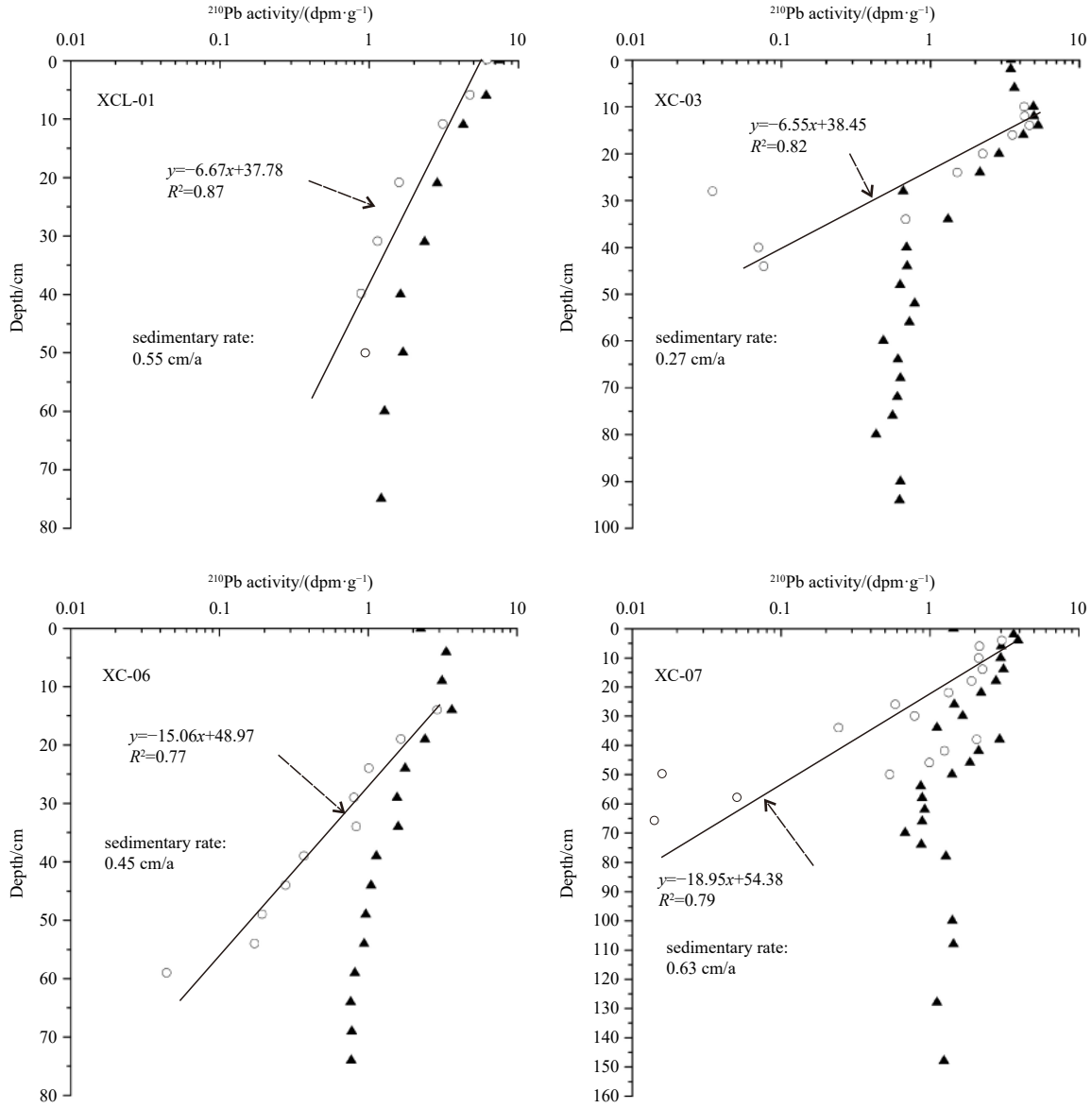


**Fig. 2.** Activity–depth profiles of $^{210}$Pb activity in the sediment cores. The dark triangle represents the total $^{210}$Pb activity, while the circle denotes the excess $^{210}$Pb activity. 1 dpm/g≈16.67 Bq/kg.

tion rate with the $^{137}$C dating method. The sedimentation rates of Core XC-08 was then calculated to 0.5 cm/a according to the average value of other four core $^{210}$Pb dating results. Base on the modern average sedimentation rate and the length of the four cores (Fig. 2; Table S1), the periods of cores XCL-01, XC-03, XC-06, XC-07 and XC-08 would be calculated to 203 a (1903 CE), 348 a (1665 CE), 266 a (1747 CE), 117 a (1896 CE), and 186 a (1827 CE), respectively.

#### 4.2.2 *Pb markers*

Aquaculture sewage is a waste material of aquaculture activities along the coasts of Hainan Island, especially in barrier-lagoon systems. Plumbum (Pb) has widely been used to detect the initial time of industrialization (e.g., Hu et al., 2013; Mo et al., 2019). Regional surveys showed that natural levels of Pb on the Hainan Island were around $25 \times 10^{-9} - 30 \times 10^{-9}$ for coastal sediments (Zhao and Yan, 1993). The Pb contamination of the Hainan Island coastal surface sediments related to the local marine aquaculture has been documented in the Xincun Lagoon (Chen et al., 2014) and many other bays and estuaries of the Hainan Island (Hu et al., 2013; Mo et al., 2019). According to historical documents, large scale mariculture in the Xincun Lagoon started around 1975–1985 CE (*Hainan Statistical Yearbook*, 1957–2013). An abrupt increase in Pb concentration was observed at about 20 cm (Fig. 3) within Core XCL-01 and, thus, assigned a date of 1980±5; therefore, we could obtain the sedimentation rate of XCL-01, which was about 0.57 cm/a. This estimate was in good concordance with the results of $^{210}$Pb dating method (0.55 cm/a).

### 4.3 *Grain size*

The mean grain size of surficial sediments ranged from 4 μm to 441 μm (Fig. 4), with an average of 44 μm. The dominate clay-silt was distributed in the central tidal basin, while sand fractions were mainly distributed in shallow water zones around the tidal basin (especially in the southeastern basin).

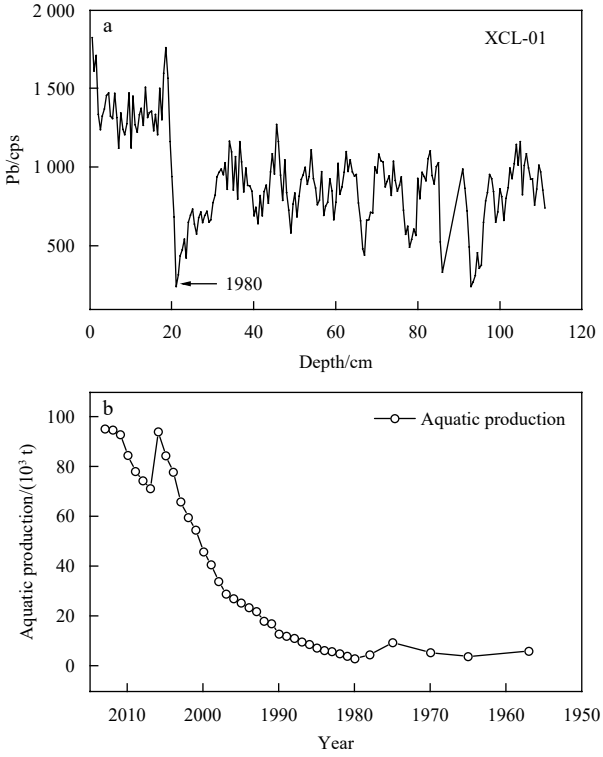


**Fig. 3.** XRF-derived bulk Pb concentration for Core XCL-01 (a), and changes of aquatic production in Lingshui City (data from the *Hainan Statistical Yearbook* for 1957–2013) (b).

The grain size standard deviation method was used to detect a representative population of grains with the highest variability (Fig. 5a). According to the diagram of the standard deviation of particle diameters (Fig. 5a), two significant populations, based on all cores, could be distinguished, i.e., <25 μm and >90 μm (coarse population). The fine-grained component can be recognized as the background deposition in the Xincun Lagoon (Zhou et al., 2017a), and the coarser-grained component corresponds to a high-energy event deposition (Sabatier et al., 2008). All cores also showed significant coarse grain peaks (100–1 000 μm) in some sand layers, and fine grain peaks (2–100 μm) in normal deposition layers (Figs 5b–f). Because the background sedimentation showed a silt facies in the tidal basin (Fig. 4), we used the coarser fraction (values of high peaks in the D90 grain size) to outline high-energy events (Fig. 6).

The D90 grain size distribution of the samples was used as a major proxy for differentiating the storm deposits from other similar environments (Boldt et al., 2010; Brandon et al., 2013; Maio et al., 2016). During the past 100 years, the D90 fraction between the five cores showed numerous grain size peaks (Fig. 6). Within Core XCL-01, the D90 grain size displayed high fluctuations, with pronounced peaks occurring around 55 cm, 52 cm, 48 cm, 40 cm, 35 cm, 30 cm, 22 cm, 20 cm, 18 cm,14 cm, 12 cm, and 5 cm (Fig. 6). In Core XC-06, the mean D90 grain size was 318 μm. The depth evolution of the D90 grain size showed six peaks at the depths of 12 cm, 22 cm, 25 cm, 35 cm, and 45 cm over the past 100 years. In Core XC-07, the D90 grain sizes only displayed three peaks at the depths of 6 cm, 18 cm, 24 cm, 30 cm, 37 cm, and 48 cm. In Core XC-08, only two main D90 grain size peaks could be observed at the depths of 27 cm and 43 cm. In Core XC-03, seven peaks were located at the depths of about 2 cm, 6 cm, 20 cm, 25 cm, 27 cm, 29 cm and 31 cm.

### 4.4 *Geochemistry*

To geochemically trace storm deposits, the inter-element ratio of given and conservative elements can be used (Dezileau et al., 2011; Raji et al., 2015). In addition, the use of inter-element ratios has the advantage of being insensitive to sample inhomogeneity and surface roughness (Richter et al., 2006; Sabatier et al., 2012). In this study, we considered the ratios of Sr/Fe and Zr/Al as further proof of high-energy storm events in Core XCL-01. High Zr/Al ratio peaks are due to coarse-grained marine sand (with rich heavy minerals; Zr), while high Sr/ Fe ratio are due to the enrichment of Sr in marine sand and shell or algal materials. Figure 7 shows that the Sr/Fe and Zr/Al ratios displayed similar variations to the D90 grain size, especially in the top 1 m of the sediment core (Fig. 7). Therefore, the geochemical results further confirmed the reliable identification of storm events by grain sizes.

### 4.5 *Hydrodynamic parameters under storm conditions*

The model results were verified using the observed tidal water level and wave height. Figure 8 shows that the Delft3D simulation results well matched the measured tidal water level and wave height. During the passage of Typhoon Doksuri, high waves and high tidal water levels were synchronous with the peak bottom shear stresses within the lagoon (Fig. 9).

The bed shear stress ($\tau$) determined by Delft3D model at the five core sites was in the range of 0.05–0.31 Pa (average, 0.08 Pa)

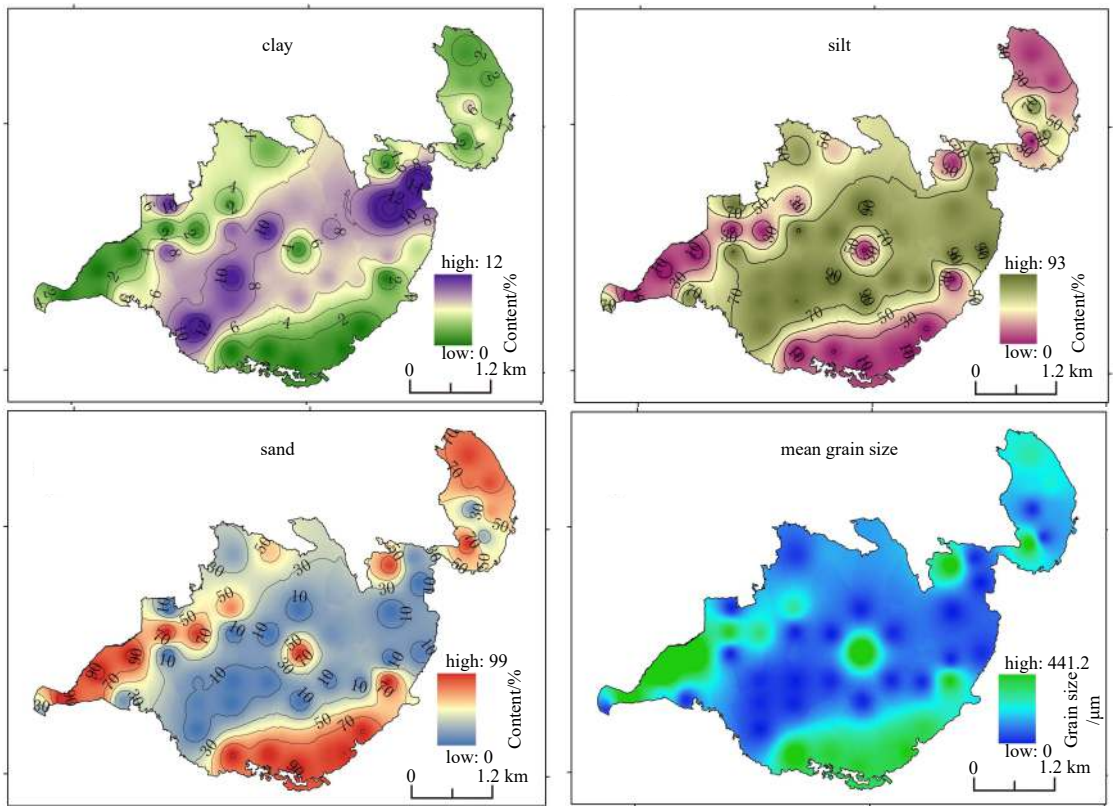


**Fig. 4.** Grain size parameters of surface sediment samples (adopted from Yang et al. (2017)).

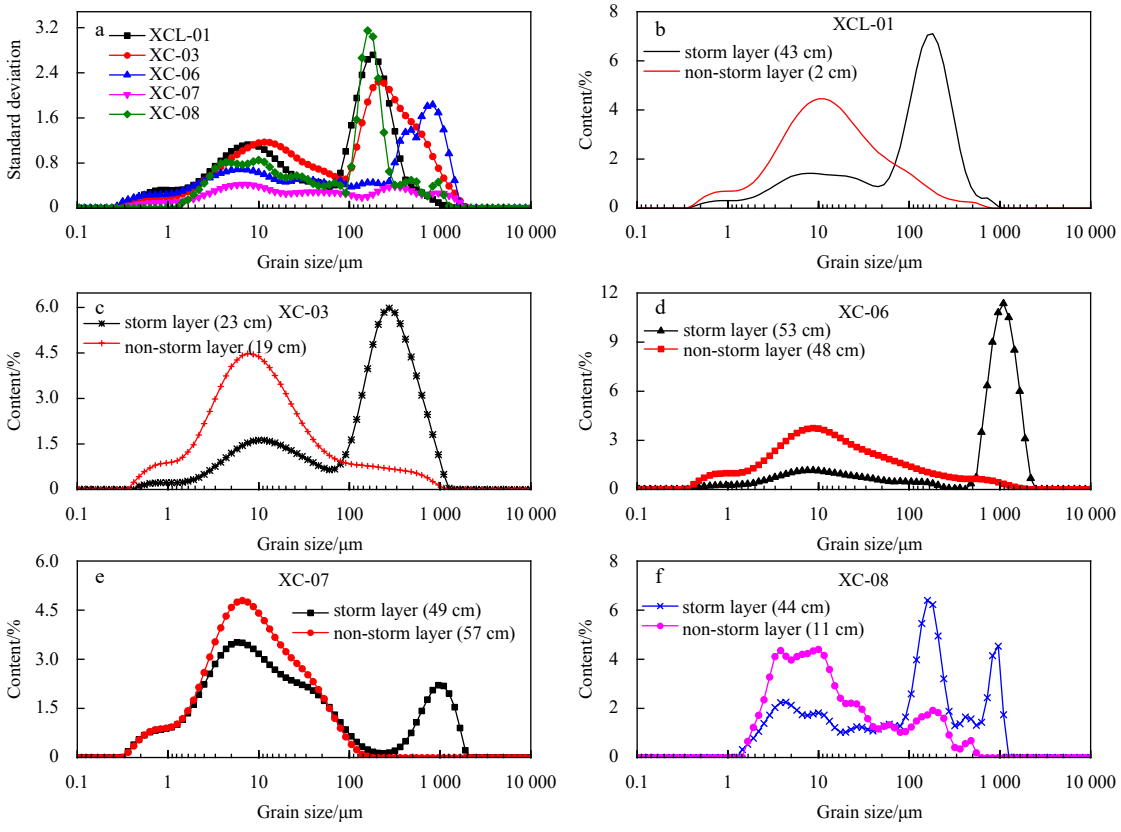


**Fig. 5.** Standard deviation vs grain size diagram for all cores (a), and grain size distribution of storm deposits and non-storm deposits of all cores (b–f).

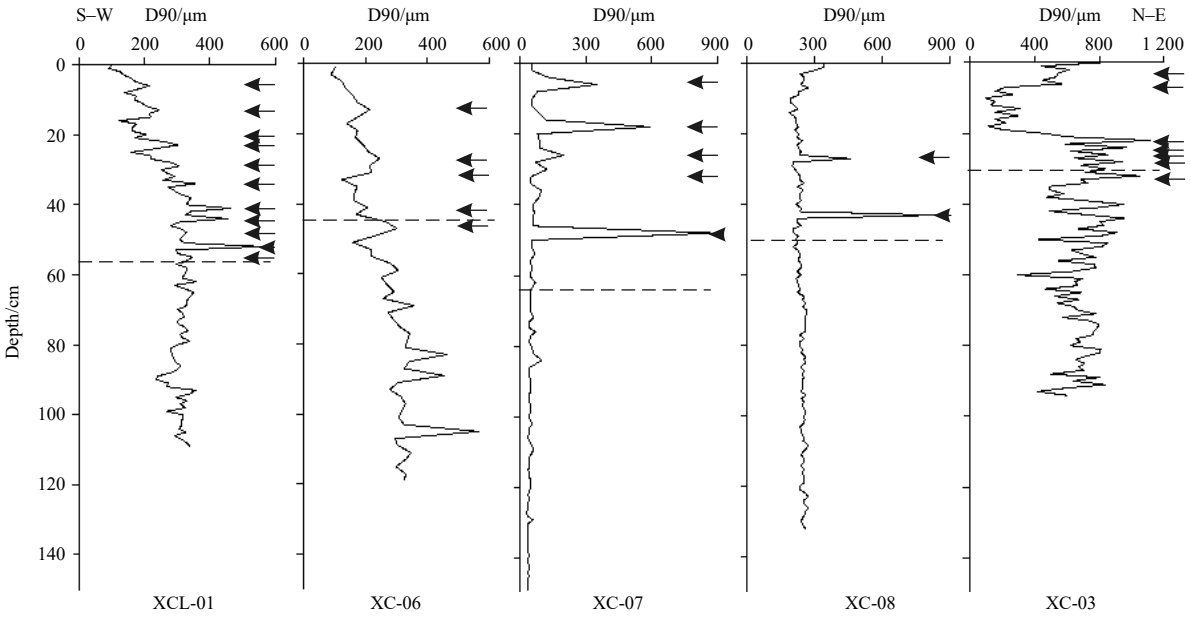


**Fig. 6.** Vertical variations in D90 grain size of cores XCL-01, XC-06, XC-07, XC-08, and XC-03. The arrows represent storm events and the dash lines represent the age of 1910 CE based on the sedimentation rate of each core. The dashed line represents the background values.

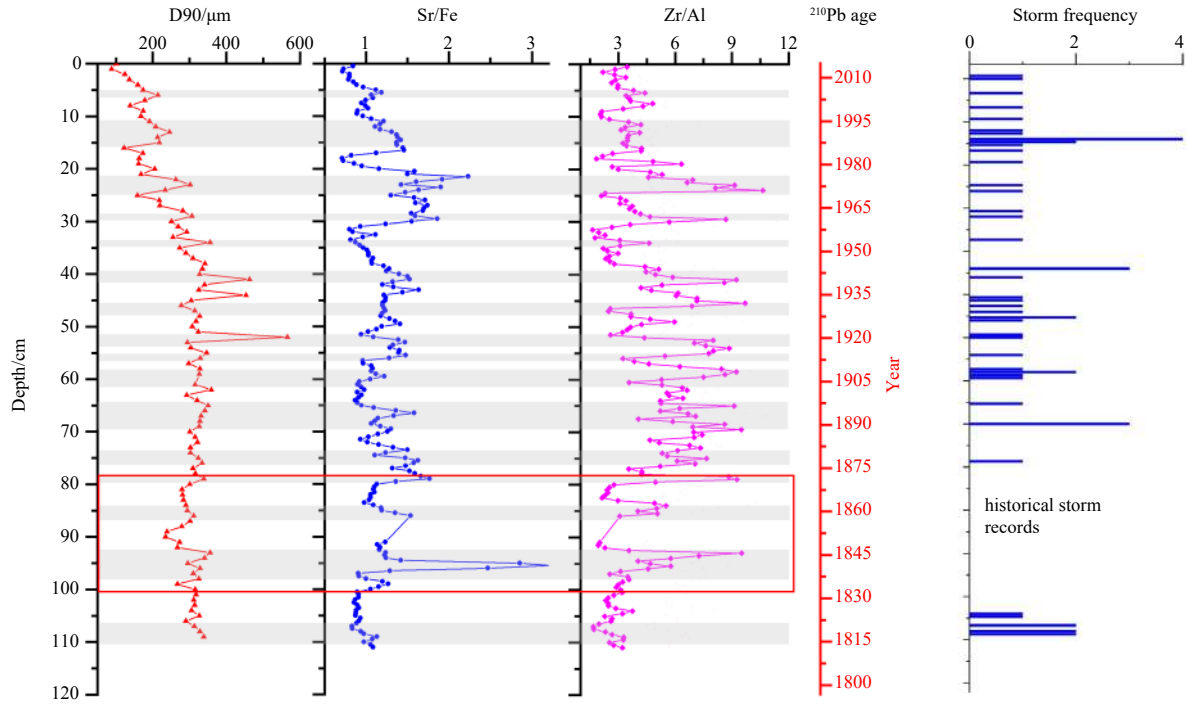


**Fig. 7.** Vertical profiles of D90 grain size and ratio of Sr/Fe and Zr/Al for Core XCL-01 as well as historical storm records of southeastern Hainan Island for post-1 800CE.

during the peak of Typhoon Doksuri, while $\tau$ was less than 0.02 Pa (average, 0.01 Pa) during normal tidal conditions (Fig. 9), indicating that the storm-averaged $\tau$ values were more than eight times higher than those during normal tidal conditions (Fig. 9). Figure 9 shows that $\tau$ values significantly differed at the five core sites during the peak of Typhoon Doksuri. The shallowest XC-03 site had the biggest $\tau$ values, being in the range of 0.03–0.31 Pa (average, 0.15 Pa). At the sites of cores XC-06, XC-07 and XC-08, the maximum $\tau$ values were estimated to be 0.16 Pa (average, 0.06 Pa), 0.24 Pa (average, 0.08 Pa), and 0.23 (average, 0.10 Pa), respectively. The deepest XCL-01 site had the smallest $\tau$ values, with the maximum critical shear stress of 0.14 Pa and an average $\tau$ value of 0.04 Pa.

## 5 Discussion

### 5.1 *Mechanism of storm deposits formation during storm passage*

To determine the storm deposit formation of the Xincun La-

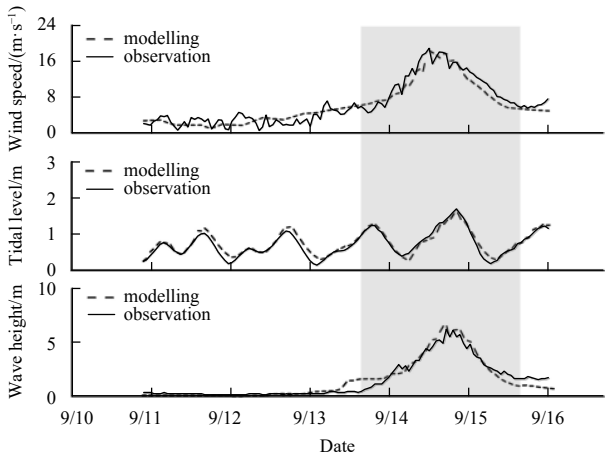


**Fig. 8.** Measured and simulated tidal water level (B1 site) and significant wave height (B2 site) in the Xincun Lagoon in 2017. The gray band represents the Typhoon Doksuri period.

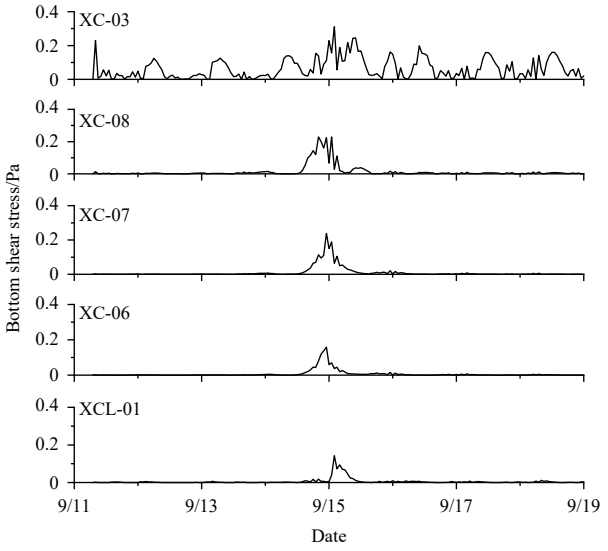


**Fig. 9.** Modeled bottom shear stress under combined current-wave action in 2017.

goon during storm passage, we analyzed the bottom shear stress. Because the bed sediment would be resuspended and transported when the bed sediment shear is smaller than the shear stress generated by storms waves and currents. We determined the $\tau_c$ value for cohesive sediment (e.g., normal tidal deposits) based on the recommendation of Taki (2001):

$$\tau_c = 0.05 + \beta \left\{ \frac{1}{\left[ \left( \frac{\pi}{6}(1+sW) \right)^{1/3} - 1 \right]} \right\}^2 , \quad (1)$$

$$s = \frac{\rho_s}{\rho_w}, \quad (2)$$

where $\tau_c$ represents the critical shear stress, $\rho_s$ is the sediment particle density (1 806 kg/m³ in this study), $\rho_w$ is the density of water (1 024 kg/m³ in this study), the electrochemical anchorage coefficient $\beta$ was set to 0.3, $s$ is the specific weight of a particle, and $W$ is the water content of the sediment. The calculated critical shear stresses of the surface sediments (e.g., normal tidal deposits) were 0.14 Pa (XCL-01), 0.17 Pa (XC-03), 0.13 Pa (XC-06), 0.13 Pa (XC-07), and 0.16 Pa (XC-08), respectively.

We determined the $\tau_c$ value for non-cohesive sediments (e.g., storm deposits) following Shield (1936):

$$\tau_c = \theta \rho g d (s-1) , \quad (3)$$

where $\theta$ is the dimensionless threshold Shields parameter, $\rho$ is the seawater density (1 030 kg/m³), $g$ is the gravitational acceleration (9.8 m/s²), $s$ is the density ratio of sediment to seawater ($s = \rho_s/\rho_w$), $\rho_s$ is the sediment particle density (2 650 kg/m³ in this study), and $d$ is the diameter of non-cohesive sediment particles (116 μm, 126 μm, 121 μm, 132 μm and 145 μm at cores XCL-01, XC-06, XC-07, XC-08, and XC-03, respectively). The calculated critical shear stresses of the non-cohesive sediments (e.g., storm deposits) were 0.20 Pa (XCL-01), 0.26 Pa (XC-03), 0.21 Pa (XC-06), 0.22 Pa (XC-07), and 0.23 Pa (XC-08), respectively.

Figure 9 shows that the bed shear stress under normal weather conditions at the five core sites was below 0.02 Pa, which was significantly smaller than the critical shear stress of both the cohesive and non-cohesive sediments. These results indicate that the sediments at the five sites could not be suspended under normal weather conditions.

Under storm conditions, taking Typhoon Doksuri as an example, the model results show that bottom stresses at the XCL-01 site during the peak of Typhoon Doksuri reached 0.14 Pa (Fig. 9), which was much less than the $\tau_c$ value of non-cohesive sediments (e.g., storm deposits; 0.20 Pa). Similar to the XCL-01 site, the modeled maximum bed shear stress at the XC-06 site (water depth about 6 m) was 0.19 Pa, which was greater than the critical stress for cohesive sediment but smaller than the critical stress for non-cohesive sediments for initial erosion. At depths less than 3 m (XC-03 site), the storm-generated shear stresses were greater than 0.3 Pa, much larger than the critical shear stress for the erosion of both cohesive and non-cohesive sediment. Even at the depth of cores XC-07 and XC-08 (about 5 m), the maximum current velocity was about 0.3 m/s (Fig. S1), and the storm-generated shear stresses at bottom bed were about 0.24 Pa and 0.23 Pa respectively. This was still larger than the calculated critical shear stresses for the erosion of both cohesive and non-cohesive sediments. Previous studies have reported that the threshold velocity for the movement of sandy sediments in the northern part of SCS is ~0.2 m/s (Tian et al., 2016), which is smaller than the velocities induced by Typhoon Doksuri in most of the shallow water areas within the Xincun Lagoon (Fig. S1).

Clearly, in shallow water areas (e.g., XC-03, XC-07, XC-08), these storm-generated shear stresses were sufficient to cause a substantial of bottom sediment erosion (of both cohesive and non-cohesive sediments) and to suspend the bottom sediments. In addition, Fig. S1 indicates that the current speed reached up to approximately 0.2 m/s in the shallow water areas during the peak of Typhoon Doksuri. Therefore, coarse sand in the sea-bed of shallow water areas may easily suspend and be transported in storm wind around 20 m/s (Typhoon Doksuri), especially near the sites of cores XC-07, XC-08, and XC-03. This indicates that the formation of storm deposits by erosion processes may also be associated with storm impacts in shallow water areas. In relatively deep-water areas (e.g., XCL-01), the storm-generated shear stresses were only sufficient to cause the erosion of cohesive sediments, but of non-cohesive sediments. This suggests that storm deposits (coarse-grained deposits) in deep areas (especially in

the southern tidal basin of Xincun Lagoon) are less likely to be eroded and longer preserved (e.g., storm deposits) than those in shallow water areas during storm passage.

Based on the sedimentary, historical, and modeling data, it appears that storms played a significant role in producing the sand horizons in the cores. We infer that during storm passage, the primary sources of sand entering the tidal basin can be summarized as follows. For Core XCL-01, coarse sand likely arrived from shallow flood tide deltas and near shore beaches along the southern shorelines. During the peak of Typhoon Doksuri, the current velocities in the tidal inlet, flood tide delta area and southern nearshore areas reached to >0.5 m/s (Figs 9 and S1), which are capable of causing a significant erosion of adjacent nearshore and flood tide delta areas, entraining sand in the eastward moving currents and southwestward moving currents, respectively (Figs 10 and S1). When these currents override shal-

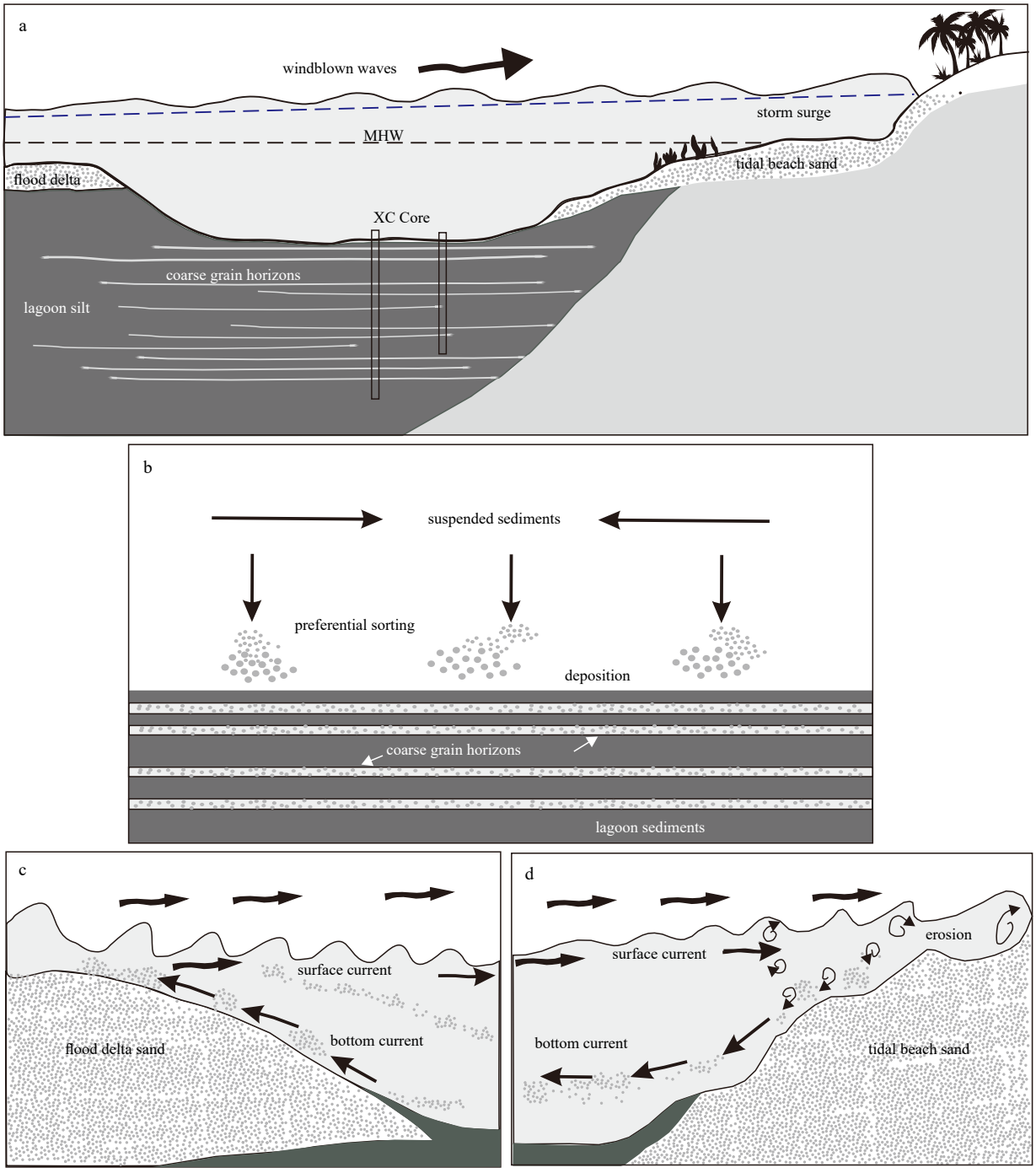


**Fig. 10.** Conceptual model of mechanisms of coarse-grained sand formation caused by storm impacts within the Xincun Lagoon sequence (modified from Maio et al., 2016). a. Conceptualized cross section of the tidal basin showing core locations, beach, and flood delta sands. Windblown waves generated by storms further increase the tide level and current speed, resulting in erosion of the flood delta, beach, and shoreface sand. b. Coarse-grained sand is suspended and transported into the tidal basin it is sorted and deposited on the tidal basin bottom bed. c and d. Increased storm surged water within the tidal basin provides up the conditions for a strong current capable of transporting sand from the flood delta tidal beach down into the tidal basin.

low areas, additional sand grains are suspended and transported westward or northeastward into the southern tidal basin near the site of Core XCL-01. For cores XC-07 and XC-08, coarse sand likely arrived from the shallow flood tide deltas (under a northward flow of around 0.1–0.3 m/s) and the north shoal areas (under a southwestward flow of around 0.05–0.2 m/s). For Core XC-03, coarse sand more likely eroded from nearshore areas along the eastern and northern shoreline under northward-southward (maximum 0.30 m/s) and eastward flow (maximum 0.35 m/s), respectively (Figs 10 and S1). For Core XC-06, coarse sand more likely eroded from the flood tide delta and north shoal bar areas under an eastward flow (Figs 10 and S1).

When quantifying the hydrodynamic processes that have deposited these coarse-grained sands based on the Typhoon Doksuri hydrographic data, it is critical to point out that the typhoon was decreasing to a tropical storm when passing by more than 100 km south of Hainan Island. Since the intensity of this storm was smaller than that of most historical major storms impacting the Xincun Lagoon (Table 1), we can assume that storms with a similar magnitude (e.g., wind, surge, and wave) to Typhoon Doksuri would deposit a coarse-grained sand bed.

### 5.2 *Proxies anomalies and storm events*

According to the sediment dynamics results (Section 5.1), coarse-grained deposits within the five cores could not have been deposited under normal tidal conditions but were carried rather by wave-current interactions during a high-energy storm event. Based on the grain size analysis, sedimentary features, and geochemical data, we detected the coarse-grained layers deposited during a storm in the lagoon sequence (e.g., Donnelly and Woodruff, 2007; Woodruff et al., 2009; Dezileau et al., 2011; Raji et al., 2015). With few exceptions, significant peaks were reflected in the D90 grain size (Fig. 6), which is similar to the results of previous studies of storm-induced deposition within back-barrier lagoons. The high content of the D90 grain size within these sand layers suggests the occurrence of increased hydrologic deposition events, indicating perturbations of extreme hydrodynamics caused by storms or intense storms (Figs 6 and 7).

To test the archives of past storms preserved in the high-barrier lagoon deposits, we identified whether the chronology of proxy anomalies corresponded to that of the history of storms impacting this region. To determine which possible historical storms produced coarse-grained layers, we combined the depth of these layers and previously defined sedimentation rates.

For the cores in the north basin area (XC-06, XC-07, XC-08, XC-03), a fewer number of positive coarse-grain anomalies for each core were identified, and many documented storm events were missing (Fig. 11). This absence of storm events was attributed to the shallower water depth and frequent perturbations by later storms.

In the southern basin, the coarse-grained sediments were mainly sourced from the southern beach sand and flood tidal delta area, based on the modeling results and sedimentary data in this study (Figs 4, 10 and S1; Section 5.1; Zhou et al., 2019). These coarse-grained sediments were very different from the mud-dominated ambient sediment near Core XCL-01 (Figs 4 and 10), which made it possible to identify these event layers in deep water areas. For Core XCL-01, we used both grain size and high-resolution XRF element ratio (Sr/Fe and Zr/Al) analysis to accurately detect every storm layers. The age of high peaks corresponded well with the documented intensive storms (Fig. 11). The first positive anomaly peak in Core XCL-01 occurred between 5 cm and 6 cm (around 2005), which corresponded to Typhoon Damrey (category 1). The absence of intense storm events between 2005 and 2015 was likely associated with a depth close to the surface and intensive human activities. Four of the largest storm tidal water levels recorded in historical documents at the Xincun Lagoon were 3.21 m (November 16, 1897), 2.44 m (May 11, 1954), 2.69 m (October 9, 1971), and 2.73 m (June 4, 1981) (Chen, 1992). Event beds among 64–67 cm (1893–1899 CE), 34 cm (1953 CE), 22–24 cm (1971–1975 CE), and 17–18 cm (1982–1984 CE) may relate to the four intense storm events including a nameless storm

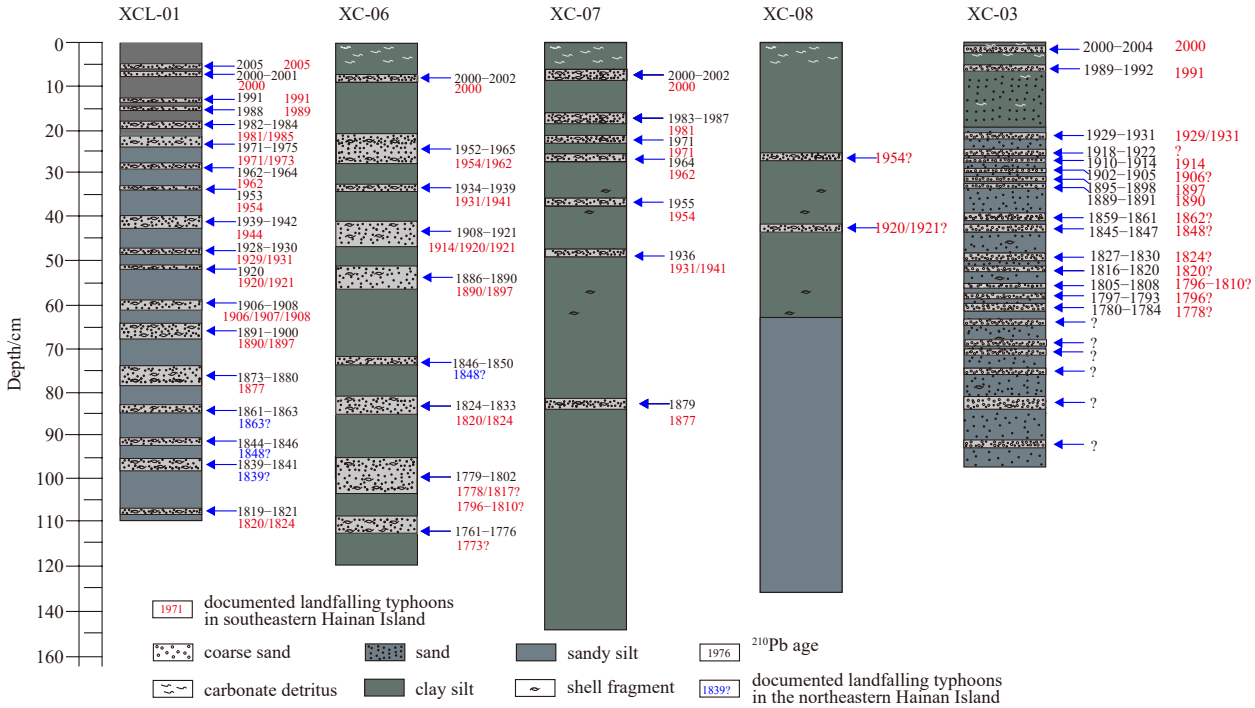


**Fig. 11.** Comparison of sedimentary storm records with historical documents.

in 1897, Typhoon Elsie (1954), Typhoon Elaine (1971), and Typhoon Kelly (1981). It should be noted that three significant anomaly peaks (84–85 cm, 93–94 cm, and 95–96 cm) could not be correlated to any documented storm event in the southeastern Hainan Island because there was no documentary record of storm events around 1830–1875 CE (Fig. 6). That these storm events were not compiled in the literature may be due to wars and social unrest during the late Qing Dynasty (e.g., the Taiping Rebellion in 1853–1864 CE; the Opium War in 1840–1860 CE). In addition, some of the missing storm event records in those periods have been documented in literature from adjacent regions (Table 2). For instance, the storm of November 1863 (shift from northwest to southeast), caused the destruction of numerous buildings and the death of thousands of people in Qiongshan County (part of Haikou City) and was considered as one of the most catastrophic events in the Hainan historical period (Chen, 1995; Table 2). Given the southeastward movement and the severity of this event, we have reason to believe that this storm passed the study area, and the information of its impact was preserved in the Xincun Lagoon sequence.

**Table 2.** Supplementary documented literature of storm events occurring in 1863, 1848, and 1939 CE

| Date | Documented description | Landfall site |
|---|---|---|
| 1863 | On November 21st in 1863 CE, *jufeng* moved from east to south, buildings were razed. On November 27th in 1863 CE, *jufeng* moved from northwest to southeast, numerous houses were destroyed, thousands of people were drowned by the storm surge, which caused hazards that have never been seen before. | Qiongshan |
| 1848 | On November 23rd in 1848 CE, a number of buildings and trees were demolished by extraordinarily strong winds. | Dingan |
| 1839 | On December 7th–18th in 1839 CE, 6 storms and floods occurred continuously, allcrops were drowned and a large number of people lost their home, which contributed to a famine that led to the death of numerous people. In the next two years (1840 and 1841 CE), corps were destroyed again by frequent floods and drought, famine was the result. | Dingan, Wenchang |

Some smaller grain size peaks at the depth of 104–108 cm may have been preserved from earlier storms in historical time (around 1815–1825 CE). This coarse-grained bed was likely related to the frequent storm period of 1817–1824 (at least seven storm events were documented in Chen (1995); Fig. 6). Moreover, some coarse-grained beds in the prehistoric sediments may be associated with a series of storm events occurring during one year or 2–3 years in a row (e.g., the event beds at the depth of 59–61 cm), while some coarse-grained event beds may relate to one or two large storm events (e.g., the event beds at the depth of 65–68 cm).

### 5.3 *Site potential for storm event reconstruction*

The accurate reconstruction of paleostorm event sequences rely on the sensitivity of a site to storm impacts (Hippensteel et al., 2013; Maio et al., 2016). The paleostorm sensitivity of a back-barrier lagoon depends on many factors (e.g., sea level, sediment supply, hydrodynamic environment, morphology dynamics, and storm frequency; Scileppi and Donnelly, 2007; Sabatier et al., 2012; Woodruff et al., 2009).

Sea-level rise could be ruled out for our study site. During the past 1 600 years, no obvious sea-level fluctuation (< 1 m) has been recorded for the Hainan Island (Zong, 2004; Jiang et al., 2018). The abrupt increase in coarse-grained event layers since around 1815 CE (Fig. 11), thus, could not be explained by the impact of sea levels.

A change of the tidal inlet position can also affect the sensitivity of a particular area to storm-induced deposition. Remote sensing and hydrodynamic survey data acquired since the 1980s clearly show that the tidal inlet of Xincun Lagoon is relatively stable (Gong et al., 2008). Furthermore, the inlet is confined by rocky strata associated with the Nanwan Hill (Fig. 1), and thus, the entrance width could have basically remained unchanged, although the main ebb tidal channel has a cyclical evolution (Gong et al., 2008). This influence is supported by the previous geological and geomorphological surveys in the Xincun Lagoon (Song, 1984; Zhao et al., 1999).

The Xincun Lagoon is a small tidal inlet system with small runoff and sediment inputs. Weak tidal currents are the main dynamic forcing in the lagoon with the current velocity over the tidal basin less than 0.1 m/s (Gong et al., 2008), suggesting that tidal current is incapable of initiating coarse-grained deposits in the tidal basin under normal conditions (Yang et al., 2017). Thus, it is likely that the increases in grain size at the present study site were caused by storm currents and waves during storm passage. In addition, the modeling results showed that the current velocity changed greatly with varying storm wind direction and water depth (Fig. S1). As the water currents turn around when reaching the shore (Figs 9 and S1), the direction of suspended sediment transport was contrary to that of the bottom sediment transport flow (Fig. 9). The erosion degree of seabed sediments would increase with an increase in the storm wind magnitude and a decrease in water depth (Fig. 9; Section 5.1). During storm passage through the Xincun Lagoon, the storm current would erode the coarse-grained sediments from the inlet or flood/ebb delta and nearshore beach and transport them into the inner part of the tidal basin (Fig. 9; Section 5.1), so that storm deposit beds would be formed (Figs 9 and 10).

Flood events may be an additional cause for the deposition of coarse-grained deposits. However, only two significant grain-size populations were separated from the cores (Fig. 5a), indicating that sediment deposition in this lagoon was dominantly controlled by two hydrodynamics. Zhou et al. (2017a, b, 2019) proved that the coarse grains were mainly from marine sources. In addition, the long distance between the river mouth and core site can significantly reduce the deposition of coarse-grained particles carried by the river to the core site. Furthermore, the small discharge of two streams in the study area make it difficult to transport large amounts of sediment (Zhou et al., 2019). Therefore, the increase in coarse-grained deposits in these cores cannot be explained by river flooding events.

Given the very small fluvial effects, the microtidal situations, and the relative stable sedimentary environment, this lagoon (at least part of the lagoon) was favorable for trapping coarse-grained sediments into this lagoon. Based on the $^{210}$Pb and Pb pollution chronologies, at least 20 coarse-grained storm events were detected in the five cores. However, the number of historic event beds within these cores was not consistent (Fig. 11), suggesting that these cores may reflect different potentials for the preservation of storm deposits due to different sensitivities to

storm impacts, coarse-grained sources, and transport pathways. After comparison with the historically documented storm records, found that Core XCL-01 was the only core that contained a relatively complete record of storm events (Figs 7 and 11). For example, during the past 100 years (since 1915), about 19 storms were recorded in Core XCL-01, which account for about 2/3 of the documental records (32, Fig. 7). This indicates that the potential for the preservation of storm deposits in the southern basin appears to be higher than that of the northern shallow water areas. The possible reason for this was the proximity to coarse-grain sources (inlet, flood delta), the southern hill block, and relatively deep water. These factors caused coarse-grained storm deposits to be more easily transported into the southern part of the basin, letting smaller storms with weaker currents transport coarse sediments to the XCL-01 site. In addition, the relatively deeper water and weak current due to the hill block in the southern basin may effectively reduce sediment resuspension under storm conditions. Although the XC-03 site seemed to be sensitive to both tropical and extratropical storms (Fig. 11), the variable sediment sources and strong resuspension complicated the calculation of an accurate storm age and the determination of storm frequency and intensity through time.

Information of paleostorm events extracted from sediment sequences can be affected by many factors (e.g., coastal geomorphology dynamics, sea level variations, sediment supply, inlet movement). However, the good agreement between historically documented major storms and the storm deposit record in the southern basin zone indicate that the Xincun Lagoon has high potential to preserve coarse-grained storm deposits related to intense storms impacting on the study area. Furthermore, the relative stable sea level rise and geomorphological environment during the past several thousand years (The Compile Committee of China Bay Records, 1999; Zong, 2004; Jiang et al., 2018) suggest that the high-barrier lagoon may have the high potential for long-term storm depositional sequence reconstruction.

## 6 Conclusions

The present study attempts to investigate sediment dynamics during storm passage and to examine the potential to reconstruct long-term storm frequencies in a high-barrier lagoon (e.g., Xincun Lagoon). Sedimentary data, hydrodynamic modeling results, and historical document records show that this high barrier lagoon was frequently and heavily affected by storm events. During storm passage, waves and currents led to suitable conditions for suspension and transport of coarse sand into the tidal basin of the lagoon, giving this lagoon a high potential to preserve storm-induced sedimentation. The sediment records cores taken in the study site recorded different sediment dynamics during storm passage. Average sedimentation rates calculated by using the $^{210}$Pb method are yield to between 0.27 mm/a and 0.63 cm/a for all cores. Base on the $^{210}$Pb dating results and Pb pollution chronostratigraphic markers, the periods of the storm deposit sequences of the cores were calculated to 203 a, 348 a, 266 a, 117 a, and 186 a, respectively. Varying geomorphologic conditions and sediment transport mechanisms caused this inconsistency of storm events among the cores, as recorded by coarse-grained sediments. However, the good agreement between historical major storms and the storm deposits recorded in the southern basin zone indicates that high-barrier lagoon may have a high potential for the long-term reconstruction of storm depositional sequences.

The paleostorm records preserved in sedimentary sequences are often incomplete and site-dependent. More efforts are needed to examine known events in various environments and sedimentation areas. Additionally, the selection of study sites and core positions are critical in the high-barrier lagoons, and a series of factors should be adequately considered, including storm pathways, storm frequency, storm deposit sources, and sediment dynamic.

***Acknowledgements***

We thank those who helped us in the field work, especially Yong Yin, Chendong Ge, Peihong Jia, Jiayu Tu, Danan Wang and Baoming Yang who were there for all the cores. Xin Fang from Second Institute Oceanography of Ministry of Natural Resources was also thanked for providing the hydrological data. Jianhua Gao helped us with some grain size technical problems.

## References

Almeida L P, Vousdoukas M V, Ferreira Ó, et al. 2012. Thresholds for storm impacts on an exposed sandy coastal area in southern Portugal. Geomorphology, 143–144: 3–12, doi: 10.1016/j.geomorph.2011.04.047

Appleby P G, Oldfield F. 1978. The calculation of lead-210 dates assuming a constant rate of supply of unsupported $^{210}$Pb to the sediment. Catena, 5(1): 1–8, doi: 10.1016/S0341-8162(78)80002-2

Bastidas L A, Knighton J, Kline S W. 2016. Parameter sensitivity and uncertainty analysis for a storm surge and wave model. Natural Hazards and Earth System Sciences, 16(10): 2195–2210, doi: 10.5194/nhess-16-2195-2016

Blott S J, Pye K. 2001. GRADISTAT: a grain size distribution and statistics package for the analysis of unconsolidated sediments. Earth Surface Processes and Landforms, 26(11): 1237–1248, doi: 10.1002/esp.261

Boldt K V, Lane P, Woodruff J D, et al. 2010. Calibrating a sedimentary record of overwash from Southeastern New England using modeled historic hurricane surges. Marine Geology, 275(1–4): 127–139, doi: 10.1016/j.margeo.2010.05.002

Brandon C M, Woodruff J D, Lane D P, et al. 2013. Tropical cyclone wind speed constraints from resultant storm surge deposition: a 2500 year reconstruction of hurricane activity from St. Marks, FL. Geochemistry, Geophysics, Geosystems, 14(8): 2993–3008, doi: 10.1002/ggge.20217

Chen Guangximg. 1992. Storms and storms in Hainan Island. Journal of China Hydrology (in Chinese), (5): 52–55

Chen Hansong. 1995. Natural Disasters in Hainan Province during the Past 1000 Years (in Chinese). Haikou: Hainan Press, 1–236

Chen Nengwang, Krom M D, Wu Yinqi, et al. 2018. Storm induced estuarine turbidity maxima and controls on nutrient fluxes across river-estuary-coast continuum. Science of the Total Environment, 628–629: 1108–1120, doi: 10.1016/j.scitotenv.2018.02.060

Chen Shiquan, Zhang Ghuangxing, Wu Zhongjie, et al. 2014. The distribution characteristics and the pollution evaluation of the heavy metals in the surface sediments of Xincun Lagoon. Transactions of Oceanology and Limnology (in Chinese), (4): 144–152

Degeai J P, Devillers B, Dezileau L, et al. 2015. Major storm periods and climate forcing in the Western Mediterranean during the Late Holocene. Quaternary Science Reviews, 129: 37–56, doi: 10.1016/j.quascirev.2015.10.009

Dezileau L, Sabatier P, Blanchemanche P, et al. 2011. Intense storm activity during the Little Ice Age on the French Mediterranean coast. Palaeogeography, Palaeoclimatology, Palaeoecology, 299(1–2): 289–297, doi: 10.1016/j.palaeo.2010.11.009

Donnelly J P, Woodruff J D. 2007. Intense hurricane activity over the past 5, 000 years controlled by El Niño and the West African monsoon. Nature, 447(7143): 465–468, doi: 10.1038/nature05834

Fogarty E A, Elsner, J B, Jagger T H, et al. 2006. Variations in typhoon landfalls over China. Advances in Atmospheric Sciences, 23(5): 665–677, doi: 10.1007/s00376-006-0665-2

Ge Chendong, Slaymaker O, Pedersen T F. 2003. Change in the sedi-

mentary environment of Wanquan River Estuary, Hainan Island, China. Chinese Science Bulletin, 48(21): 2357–2361, doi: 10.1360/03wd0152

Gong Wenping, Wang Yapin, Wang Danru, et al. 2008. Hydrodynamics under combined action of wave and tide and its implication for the sediment dynamics in Xincun Tidal Inlet, Hainan. Journal of Marine Sciences (in Chinese), 26(2): 1–12

Greening H, Doering P, Corbett C. 2006. Hurricane impacts on coastal ecosystems. Estuaries and Coasts, 29(6): 877–879, doi: 10.1007/bf02798646

Hippensteel S P, Eastin M D, Garcia W J. 2013. The geological legacy of Hurricane Irene: implications for the fidelity of the paleostorm record. GSA Today, 23(12): 4–10, doi: 10.1130/GSATG184A.1

Hu Bangqi, Cui Ruyong, Li Jun, et al. 2013. Occurrence and distribution of heavy metals in surface sediments of the Changhua River Estuary and adjacent shelf (Hainan Island). Marine Pollution Bulletin, 76(1–2): 400–405, doi: 10.1016/j.marpolbul.2013.08.020

Hu Kelin, Chen Qin, Wang Hongqing. 2015. A numerical study of vegetation impact on reducing storm surge by wetlands in a semi-enclosed estuary. Coastal Engineering, 95: 66–76, doi: 10.1016/j.coastaleng.2014.09.008

IPCC. 2013. Climate change 2013: The physical science basis. In: Stocker T F, Qin D, Plattner G K, et al. Contribution of Working Group I to the Fifth Assessment Report of the Intergovernmental Panel on Climate Change. Cambridge: Cambridge University Press

Jia Jianjun, Gao Jianhua, Liu Yifei, et al. 2012. Environmental changes in Shamei Lagoon, Hainan Island, China: Interactions between natural processes and human activities. Journal of Asian Earth Sciences, 52: 158–168, doi: 10.1016/j.jseaes.2012.03.008

Jiang Tao, Liu Xiangjun, Yu Tao, et al. 2018. OSL dating of late Holocene coastal sediments and its implication for sea-level eustacy in Hainan Island, Southern China. Quaternary International, 468: 24–32, doi: 10.1016/j.quaint.2017.11.039

Lane P, Donnelly J P, Woodruff J D, et al. 2011. A decadally-resolved paleohurricane record archived in the late Holocene sediments of a Florida sinkhole. Marine Geology, 287(1–4): 14–30, doi: 10.1016/j.margeo.2011.07.001

Li R H, Liu S M, Li Y W, et al. 2014. Nutrient dynamics in tropical rivers, lagoons, and coastal ecosystems of eastern Hainan Island, South China Sea. Biogeosciences, 11(2): 481–506, doi: 10.5194/bg-11-481-2014

Li Wenhuan, Zhu Wanli. 2001. Characteristic analysis of the storm tide and the wave caused by typhoon NO. 0016 (Wukong). Marine Forecasts (in Chinese), 18(4): 43–47

Li Ming, Zhong Liejun, Boicourt W C, et al. 2006. Hurricane - induced storm surges, currents and destratification in a semi-enclosed bay. Geophysical Research Letters, 33(2): L02604, doi: 10.1029/2005GL024992

Liang Haiping, Liang Haiyan, Che Zhiwei, et al. 2015. A statistical analysis of landfall tropical cyclone in fifty years in Hainan province. Marine Forecasts (in Chinese), 32(4): 68–74

Liu K B, Fearn M L. 1993. Lake-sediment record of late Holocene hurricane activities from coastal Alabama. Geology, 21(9): 793–796, doi: 10.1130/0091-7613(1993)021<0793:LSROLH>2.3.CO;2

Liu Xin, Wang Yebao, Costanza R, et al. 2019. Is China's coastal engineered defences valuable for storm protection?. Science of the Total Environment, 657: 103–107, doi: 10.1016/j.scitotenv.2018.11.409

Maio C V, Donnelly J P, Sullivan R, et al. 2016. Sediment dynamics and hydrographic conditions during storm passage, Waquoit Bay, Massachusetts. Marine Geology, 381: 67–86, doi: 10.1016/j.margeo.2016.07.004

Mo Ling, Zheng Jing, Wang Ting, et al. 2019. Legacy and emerging contaminants in coastal surface sediments around Hainan Island in South China. Chemosphere, 215: 133–141, doi: 10.1016/j.chemosphere.2018.10.022

Raji O, Dezileau L, Von Grafenstein U, et al. 2015. Extreme sea events during the last millennium in the northeast of Morocco. Natural Hazards and Earth System Sciences, 15(2): 203–211, doi: 10.5194/nhess-15-203-2015

Ren Fumin, Gleason B, Easterling D. 2002. Typhoon impacts on China's precipitation during 1957–1996. Advances in Atmospheric Sciences, 19(5): 943–952, doi: 10.1007/s00376-002-0057-1

Richter T O, van der Gaast S, Koster B, et al. 2006. The Avaatech XRF Core Scanner: technical description and applications to NE Atlantic sediments. Geological Society, London, Special Publications, 267: 39–50, doi: 10.1144/GSL.SP.2006.267.01.03

Rouina B B, Bassetti M A, Touir J, et al. 2016. Sedimentary and microfaunal evolution in the Quaternary deposits in El Akarit river mouth (Gulf of Gabes, Tunisia): paleo-environments and extreme events. Journal of African Earth Sciences, 121: 30–41, doi: 10.1016/j.jafrearsci.2016.05.016

Sabatier P, Dezileau L, Colin C, et al. 2012. 7000 years of paleostorm activity in the NW Mediterranean Sea in response to Holocene climate events. Quaternary Research, 77(1): 1–11, doi: 10.1016/j.yqres.2011.09.002

Sabatier P, Dezileau L, Condomines M, et al. 2008. Reconstruction of paleostorm events in a coastal lagoon (Hérault, South of France). Marine Geology, 251(3–4): 224–232, doi: 10.1016/j.margeo.2008.03.001

Scileppi E, Donnelly J P. 2007. Sedimentary evidence of hurricane strikes in western Long Island, New York. Geochemistry, Geophysics, Geosystems, 8(6): Q06011, doi: 10.1029/2006GC001463

Shield N D. 1936. Anwendung Der Ahnlickeit Mechanik under Turbulenzforschung Auf Die Geschiebelerwegung. Mitt Preoss Versuchanstalt fur Wasserbau und Schiffbau, 26

Song C J. 1984. Geomorphology and the tidal inlets in the East Coast of Hainan Island. Studia Marine Science of South China Sea (in Chinese), 5: 31–50

Switzer A D, Jones B G. 2008. Large-scale washover sedimentation in a freshwater lagoon from the southeast Australian coast: sea-level change, tsunami or exceptionally large storm?. The Holocene, 18(5): 787–803, doi: 10.1177/0959683608089214

Taki K. 2001. Critical shear stress for cohesive sediment transport. In: McAnally W H, Mehta A J, eds. Coastal and Estuarine Fine Sediment Processes. Amsterdam: Elsevier, 53–61

The Compile Committee of China Bay Records. 1999. China Bay Records 11th Fascicule (in Chinese). Beijing: China Ocean Press, 109–130

Tian Zhuangcai, Guo Xiujun, Qiao Luzheng, et al. 2016. Analysis of spatial distribution characteristics of seabed sediments critical starting velocity in the northern South China Sea. Chinese Journal of Rock Mechanics and Engineering (in Chinese), 35(S2): 4287–4294, doi: 10.13722/j.cnki.jrme.2016.0800

Wang Ying. 1998. Tidal inlets in Hainan Island coast (in Chinese). Beijing: China Environmental Science Press, 1–282

Wang Aijun, Gao Shu, Chen Jian, et al. 2009. Sediment dynamic responses of coastal salt marsh to typhoon "KAEMI" in Quanzhou Bay, Fujian Province, China. Chinese Science Bulletin, 54(1): 120–130, doi: 10.1007/s11434-008-0365-7

Woodruff J D, Donnelly J P, Okusu A. 2009. Exploring typhoon variability over the mid-to-late Holocene: evidence of extreme coastal flooding from Kamikoshiki, Japan. Quaternary Science Reviews, 28(17–18): 1774–1785, doi: 10.1016/j.quascirev.2009.02.005

Yang Yang, Gao Shu, Zhou Liang, et al. 2017. Classifying the sedimentary environments of the Xincun Lagoon, Hainan Island, by system cluster and principal component analyses. Acta Oceanologica Sinica, 36(4): 64–71, doi: 10.1007/s13131-016-0939-1

Ying Ming, Zhang Wei, Yu Hui, et al. 2014. An overview of the China Meteorological Administration tropical cyclone database. Journal of Atmospheric and Oceanic Technology, 31(2): 287–301, doi: 10.1175/JTECH-D-12-00119.1

Zhao Yiyang, Yan Mingcai. 1993. Element abundances in China shallow sea deposits. Science in China (Series B) (in Chinese), 23(10): 1084–1090

Zhao Huanting, Zhang Qiaomin, Song Chaojing, et al. 1999. Geomor-

phology and Environment of the South China Coast and South China Sea Islands (in Chinese). Beijing: Science Press, 1–528

Zheng Guangming, Tang Danling. 2007. Offshore and nearshore chlorophyll increases induced by typhoon winds and subsequent terrestrial rainwater runoff. Marine Ecology Progress Series, 333: 61–74, doi: 10.3354/meps333061

Zhou Liang, Gao Shu, Gao Jianhua, et al. 2017b. Reconstructing environmental changes of a coastal lagoon with coral reefs in Southeastern Hainan Island. Chinese Geographical Science, 27(3): 402–414, doi: 10.1007/s11769-017-0867-9

Zhou Liang, Gao Shu, Yang Yang, et al. 2017a. Typhoon events recorded in coastal lagoon deposits, southeastern Hainan Island. Acta Oceanologica Sinica, 36(4): 37–45, doi: 10.1007/s13131-016-0918-6

Zhou Liang, Yang Yang, Wang Zhanghua, et al. 2019. Investigating ENSO and WPWP modulated typhoon variability in the South China Sea during the mid-late Holocene using sedimentological evidence from southeastern Hainan Island, China. Marine Geology, 416: 105987, doi: 10.1016/j.margeo.2019.105987

Zhou Liang, Shi Yong, Zhao Yaqing, et al. 2021. Extreme floods of the Changjiang River over the past two millennia: contributions of climate change and human activity. Marine Geology, 433: 106418, doi: 10.1016/j.margeo.2020.106418

Zong Yongqiang. 2004. Mid-holocene sea-level highstand along the Southeast Coast of China. Quaternary International, 117(1): 55–67, doi: 10.1016/S1040-6182(03)00116-2

## Supplementary information:

**Fig. S1** Modeled current field within the Xincun Lagoon for Typhoon Doksuri (18:00:00 September 14, 2017).

**Table S1.** Data collection of the sediment cores.

The supplementary information is available online at https://10.1007/s13131-021-1833-z and www.aosocean.com. The supplementary information is published as submitted, without typesetting or editing. The responsibility for scientific accuracy and content remains entirely with the authors.